J Nanopart Res (2021) 23:227
https://doi.org/10.1007/s11051-021-05334-x

RESEARCH PAPER

Effective ROS generation and morphological effect of copper oxide nanoparticles as catalysts

Simbongile Sicwetsha · Sindisiwe Mvango · Tebello Nyokong · Philani Mashazi

Received: 18 May 2021 / Accepted: 24 September 2021

Abstract In this work, the successful synthesis of spherical (sCuONPs) and rod-like (CuONRs) copper oxide nanoparticles was reported. Several microscopic and spectroscopic techniques were used to confirm the different morphologies (spherical and rod-like) and also different diameter sizes. Copper metal within nanomaterials had different oxidation states (Cu^0, Cu^+, and Cu^{2+}) as was confirmed by X-ray photoelectron spectroscopy (XPS). The optical properties of the synthesized nanoparticles were investigated, and their reactive oxygen radical species (ROS) generation was confirmed using UV–vis spectroscopy. Copper oxide nanoparticles catalytically converted H_2O_2 to form ROS ($HO^{\bullet -}$, $HOO^{\bullet -}$, or $O_2^{\bullet -}$). ROS generation was confirmed using UV–vis spectroscopy and 1,3-diphenylbenzofuran (DPBF, as a radical quencher) and also using electron paramagnetic resonance (EPR) spectroscopy and 2,2,6,6-tetramethylpiperidine (TEMP) as a spin trap. UV–vis spectroscopy was further used to monitor a blue color development when copper oxide nanoparticles were mixed with 3,3′,5,5′-tetramethylbenzidine (TMB) and hydrogen peroxide (H_2O_2). The color changes were confirmed by UV–vis spectra with absorption maxima at 370 nm and 652 nm and naked eye for blue color development. Oxidase enzymes produce hydrogen peroxide as by-product and this property was used for the detection of biological analytes. Glucose and glucose oxidase (GOx) enzyme were used as model bioanalytical system.

Keywords Copper oxide nanoparticles · Anisotropic nanoparticles · Artificial enzymes · Nanozymes · Peroxidase mimetics · Glucose detection

This article is part of the topical collection: Nanotechnology Convergence in Africa, Guest Editors: Mamadou Diallo, Abdessattar Abdelkefi, and Bheki Mamba

Supplementary Information The online version contains supplementary material available at https://doi.org/10.1007/s11051-021-05334-x.

S. Sicwetsha · S. Mvango · P. Mashazi
Chemistry Department, Rhodes University, Makhanda 6139, South Africa

T. Nyokong · P. Mashazi (✉)
Institute for Nanotechnology Innovation, Rhodes University, Makhanda 6139, South Africa
e-mail: p.mashazi@ru.ac.za

Introduction

Nanomaterials of metal and metal oxides have found numerous applications due to their optical and excellent catalytic properties. In the last few decades, their excellent catalytic properties have been exploited and found to further mimic enzyme-like activity such as that of catalase and peroxidase. These enzyme-like catalysis properties allowed for their use as stable and cheap substitutes for enzymes in immunoassay

Published online: 16 October 2021

applications. Since the discovery of the peroxidase-like activity of iron oxide (Fe_3O_4) (Gao et al. 2007), ceria oxide (CeO_2) (Zhang et al. 2014), and vanadium oxide (V_2O_5) (André et al. 2011), several metal oxides have been investigated. In this research, we investigated the synthesis and characterization of copper oxide nanoparticles (CuONPs) with spherical and rod-like morphology. The synthesized CuO nanomaterials were investigated for their catalytic properties in converting hydrogen peroxide (H_2O_2) into reactive oxygen radical species (ROS). Reactive oxygen radical species oxidized chromogenic substrates such as 3,3′,5,5′-tetramethylbenzidine (TMB), 2,2′-azinobis(3-ethylbenzothiazoline-6-sulphonic acid) (ABST), and o-phenylenediamine (OPD) into colored products. This reaction was similar to the well-known horseradish peroxidase (HRP) enzyme catalysis. CuO nanomaterials are monoclinic in structure with a narrow band gap (1.9–2.1 eV) and are p-type semiconductors. They exist as either cuprous oxide (Cu_2O), cupric oxide (CuO) (Huo et al. 2014; Gao et al. 2015), or copper hydroxide $Cu(OH)_2$ (Shackery et al. 2016). The band gap for Cu_2O is between 2.1 and 2.6 eV. The conducting properties in the p-type semiconductors arise from the holes in the valence band. The advantage of CuONPs over other metal oxide nanoparticles is their low surface potential barrier, and this affects their electric field emission properties (Huo et al. 2014; Gao et al. 2010; Johan et al. 2011). CuO nanoparticles possess high catalytic activity similar to the bulk copper, but due to large surface-to-volume ratio, the nanoparticles are more efficient as catalysts. As a result, they have been in various applications such as in catalysis, gas sensing, material in batteries, heat transfer fluids, and solar energy (Huo et al. 2014; Johan et al. 2011).

Amongst the various methods used for synthesizing CuO nanomaterials, sol–gel method was most preferred and due to its simplicity (Aparna et al. 2012) and allowed for large-scale production. Sol–gel method was therefore used to synthesize spherical and rod-like CuO nanomaterials. Metals or metalloid elements surrounded by various reactive ligands are the precursors for the synthesis and formation of the colloidal solutions. Copper acetate in solution reacts with sodium hydroxide (NaOH) to produce copper hydroxide, $Cu(OH)_2$. $Cu(OH)_2$ decomposes to form copper oxide (CuO) during the heating step. The morphology and the size of the copper nanoparticles are dependent on the reaction time, pH, and capping agent (Huo et al. 2014; Gao et al. 2010; Kshirsagar et al. 2017). The availability of a larger number of nuclei at a given time induces a decrease in the nanoparticle size because smaller metal nuclei grow and consume metal ions. The pH of the aqueous solution has an influence on the progress of the copper reduction reaction. Yao et al. reported this to be due to kinetic enhancement of the nucleation rate conducive environment for a reduction in nanoparticle sizes due to enhanced nucleation rate (Yao et al. 2015). Cu metal has strong affinity for oxygen or oxygen-rich compounds and thus always forms stable metal oxides (Gawande et al. 2016). Also the nanomaterials of copper always form metal oxides when compared to inert or noble metal nanoparticles that form as purely monometallic nanoparticles. CuO nanomaterials studied in literature have focused on their preparation using electrochemical methods (Shackery et al. 2016; El-Safty and Shenashen 2020; Luo et al. 2012a; Li et al. 2010; Jiang and Zhang 2010; Reitz et al. 2008; Zhong et al. 2016). The electrochemically synthesized CuO nanomaterials allow for their deposition onto the electrode surface used and have been applied in non-enzymatic detection of glucose. The different morphologies obtained using electrochemical synthesis method include spherical (Aparna et al. 2012; Reitz et al. 2008; Zhong et al. 2016), nanosheets (Zhong et al. 2016), nanowires (Zhong et al. 2016; Ni et al. 2014), nanoflowers (Wang et al. 2010), rod-like (Shackery et al. 2016; Wang et al. 2010; Chen et al. 2013), nanocubes (Luo et al. 2012b), nanosheet arrays (Wang et al. 2011), nanotube arrays (Zhang et al. 2003; Zhou et al. 2013a), nanofibers (Wang et al. 2009), and nanobelts (Huang et al. 2009). All these different morphologies of copper oxide nanostructures were obtained as co-deposits onto conducting electrode surfaces for electrochemical studies.

In this work, a sol–gel wet chemical method was reported for the synthesis of spherical and rod-like copper oxide nanostructured materials. The synthesized CuONPs were evaluated for their potential as artificial enzymes or nanozymes. As nanozymes, CuONPs reacted with H_2O_2 in the presence of TMB as a chromogen to produce blue colored products. The steps involved the catalytic reduction of H_2O_2 to produce ROS which oxidized TMB into blue colored products with absorption maxima at 370 nm and 652 nm. The effect of shape (spherical and rod-like), morphology, and composition of copper oxide

nanoparticles on their peroxidase-like activity was evaluated. The environmental conditions of CuO nanomaterials as potential enzyme mimetics were evaluated and compared to the natural enzymes (horse-radish peroxidase enzyme). We believe this is the first time a comparative study of this nature is conducted.

Experimental

Materials and methods

Sodium citrate tribasic ($Na_3C_6H_5O_7$), horseradish peroxidase (HRP, E.C. 1.11.1.7, Type VII, lyophilized powder, 250–330 U.mg^{-1}), 3,3′,5,5′-tetramethylbenzidine (TMB), copper acetate $Cu(OAc)_2$, sodium hydroxide (NaOH) pellets, D-(+)-glucose powder, glucose oxidase (GOx, EC 1.1.3.4. from *Aspergillus niger*, Type VII), sodium acetate (NaAc), potassium dihydrogen phosphate (KH_2PO_4), 2,2,6,6-tetramethylpiperidine (TEMP), disodium hydrogen phosphate (Na_2HPO_4), and 1,3-diphenyl-isobenzofuran (DPBF) were purchased from Sigma–Aldrich. Absolute ethanol (EtOH), 30% hydrogen peroxide (H_2O_2), methanol (MeOH), and glacial acetic acid were purchased from B&M Scientific. Dimethylsulfoxide (DMSO) was purchased from associated chemical enterprises (ACE). All the reagents were of analytical grade, and all aqueous solutions were prepared using double distilled or ultrapure water with the resistivity of 18 μΩ.cm obtained from a Milli-Q Water System (Millipore Corp., Bedford, MA, USA). The buffer solutions of different pH values were prepared using buffer tablets purchased from SAARCHEM. Methanol was used to dissolve TMB and DMSO to dissolve DPBF. Phosphate-buffered solution (PBS, 0.010 mol.L^{-1}, pH 7.4) was prepared following the reported method (Song et al. 2003; Tshenkeng and Mashazi 2020) using appropriate amounts of Na_2HPO_4, KH_2PO_4, and chloride salts, dissolved in ultra-pure (Milli-Q) water. Acetate buffer solution (pH 5.0) was also prepared using a method reported in the literature (Zhou et al. 2013b). A buffer solution (pH 4.0, 2.0 mol. L^{-1}) was prepared by mixing of 82 mL of acetic acid (2.0 mol.L^{-1}) and 18 mL of sodium acetate (2.0 mol. L^{-1}).

Synthesis of spherical and rod-like copper oxide nanoparticles

Spherical copper nanoparticles were synthesized following the reported sol–gel method (Chen et al. 2012). A mixture of copper acetate aqueous solution (70 mL of 20 mmol.L^{-1}) and 0.25 mL glacial acetic acid were added into a round-bottomed flask equipped with a condenser and heated to reflux. The boiling solution was vigorously stirred. NaOH (4.0 mmol.L^{-1}, 10 mL) aqueous solution was rapidly added to the above boiling solution. A black precipitate immediately formed, and the reaction was allowed to proceed for 30 min. The warm solution was cooled to room temperature, and the precipitate was centrifuged, washed three times with absolute ethanol and dried in air at room temperature. This reaction resulted in a formation of spherical copper oxide nanoparticles, designated as sCuONPs.

Anisotropic copper nanoparticles with rod-like morphology were prepared following the same method as above with slight modification. Briefly, a mixture of copper acetate (80 mmol.L^{-1}, 75 mL) and glacial acetic acid (1.0 mL) was added into a round-bottom flask with a condenser attached. The mixture was heated to reflux with continuous stirring. NaOH (6.0 mol.L^{-1}, 10 mL) was quickly added. A black precipitate formed immediately, and the reaction continued for another 30 min. The precipitate was centrifuged, washed three times with ethanol and air dried at room temperature to yield a copper oxide nanorod, designated as CuONRs.

Peroxidase-like activity of sCuONPs and CuONRs

The investigation of the peroxidase-like activity of sCuONPs and CuONRs was conducted at room temperature using 3,3′,5,5′-tetramethylbenzidine (TMB) in the presence of hydrogen peroxide (H_2O_2). Briefly, hydrogen peroxide (50 μL, 50 mmol.L^{-1}), TMB (50 μL, 5.0 mmol.L^{-1}), and 20 μL of sCuONPs and CuONRs (100 μg.mL^{-1}) were mixed in 0.20 mol. L^{-1} acetate buffer solution (pH 5). After the addition of the nanoparticles, the evolution of a blue color was observed, and an increase in the absorption band at 652 nm was monitored using UV–vis spectrophotometer.

Reactive oxygen radical species (ROS) generation and monitoring using DPBF (UV–vis) and TEMP (EPR)

The production of reactive oxygen radical species (ROS) was investigated using 1,3-diphenylisobenzofuran (DPBF) as a radical scavenger and 2,2,6,6-tetramethylpiperidine (TEMP) as spin trap. For DPBF, the UV–vis absorption spectra were used to monitor the degradation products. For TEMP, EPR signal was used to monitor the spin trap. The experimental setup contained DPBF (50 µL, 0.25 mmol.L^{-1}) dissolved in a mixture of DMSO and H_2O in ration 1:10 (v:v). About 75 µL of hydrogen peroxide (6.0 mmol.L^{-1} for sCuONPs or 12 mmol.L^{-1} for CuONRs) was mixed with 50 µL of 100 µg.mL^{-1} of sCuONPs or CuONRs. UV–vis spectra were recorded every minute monitoring the decreasing absorption band at 417 nm. EPR experiment used to confirm the radical generation had similar concentrations as above, but DPBF was substituted with TEMP.

Glucose detection using sCuONPs and CuONRs

The first reaction was the enzymatic reaction between D-glucose and glucose oxidase (GOx) enzyme to produce D-gluconolactone and hydrogen peroxide. Briefly, GOx (50 µL, 5.0 µg.mL^{-1}) and 25 µL of D-glucose (varied concentrations) in phosphate buffer (75 µL, pH 7) were allowed to react at 35 °C. After 45 min, a 50 µL solution of 400 µg.mL^{-1} of either sCuONPs or CuONRs was added. This was followed by addition of 100 µL of TMB (4.0 mmol.L^{-1} for sCuONPs or 5.0 mmol.L^{-1} for CuONRs) in acetate buffer (0.20 mol.L^{-1}) at final optimum pH 5. The reaction was monitored using UV–vis spectrophotometer and the absorption at 652 nm.

Results and discussion

Synthesis and characterization of CuO nanoparticles

The synthesis of copper oxide nanoparticles (sCuONPs and CuONRs) was accomplished by dissolving copper acetate in glacial acetic acid, and the mixture was heated to reflux. The addition of sodium hydroxide resulted in the formation copper oxide nanoparticles. Heating the reaction is important for decomposing copper hydroxide, $Cu(OH)_2$, to form copper oxide (CuO) nanoparticles (Kshirsagar et al. 2017). When the concentration of copper acetate and sodium hydroxide were increased, copper oxide nanorods (CuONRs) formed. The TEM images confirmed the spherical morphology in Fig. 1a even though the TEM showed agglomeration. The sCuONPs morphology was similar to the previously reported spherical CuONPs (Chen et al. 2012). In Fig. 1c, rod-like morphology of nanoparticles was observed with varying sizes. The nanomaterials size distribution was 8.5 ± 2.3 nm for spherical nanoparticles (Fig. 1b). For the CuONRs, the size distribution was 11 ± 4.5 nm transverse (width) in Fig. 1d and 40 ± 5.6 nm longitudinal (length) in Fig. 1e. The powder XRD patterns, in Fig. 1f, are for both spherical and rod-like nanoparticles. The XRD patterns exhibited similar peaks at the following angles (2Θ, degrees) 32.6, 35.6, 38.8, 48.9, 53.3, 57.9, 61.5, 65.9, 67.5, 71.9, 74.5 indexed for (110), (−111), (111), (−202), (020), (202), (−113), (022), (220), (311), and (004) Miller indices. The XRD pattern fitted very well with the material from a standard card JCPDF 72–0629. The formation of rod-like copper oxide nanoparticles forms with the (111) facet growth whilst the (110) remaining the same (Chen et al. 2012).

Scanning electron microscope (SEM) and energy dispersive X-ray spectroscopy (EDS) were used to characterize (a) sCuONPs and (b) CuONRs as shown in Fig. S1 (Support Information, SI). The SEM images showed large powder particles of different sizes. The mark X in the SEM images indicates the area where EDS analysis was conducted. The semi-quantitative analysis of the EDS spectrum showed that sCuONPs in Fig. S1a had weight percent (wt %) of 32.5% for Cu, 55.9% for O, and 11.7% for C. CuONRs in Fig. S1b had 37.8% for Cu, 53.9% for O, and 8.3% for C. The carbon was from the glacial acetic used in the preparation of CuONPs. The EDS spectra showed the elemental composition (wt %) of the sCuONPs and CuONRs, but it is a semi-quantitative technique. X-ray photoelectron spectroscopy (XPS) as an analytical technique was used for elemental quantification analysis (atomic %, at %) and composition of the nanoparticles. XPS was also used to confirm the oxidation states of the various atoms present within sCuONPs and CuONRs.

The XPS survey spectra of sCuONPs, Fig. 2a, and CuONRs, Fig. 2a', showed elements corresponding

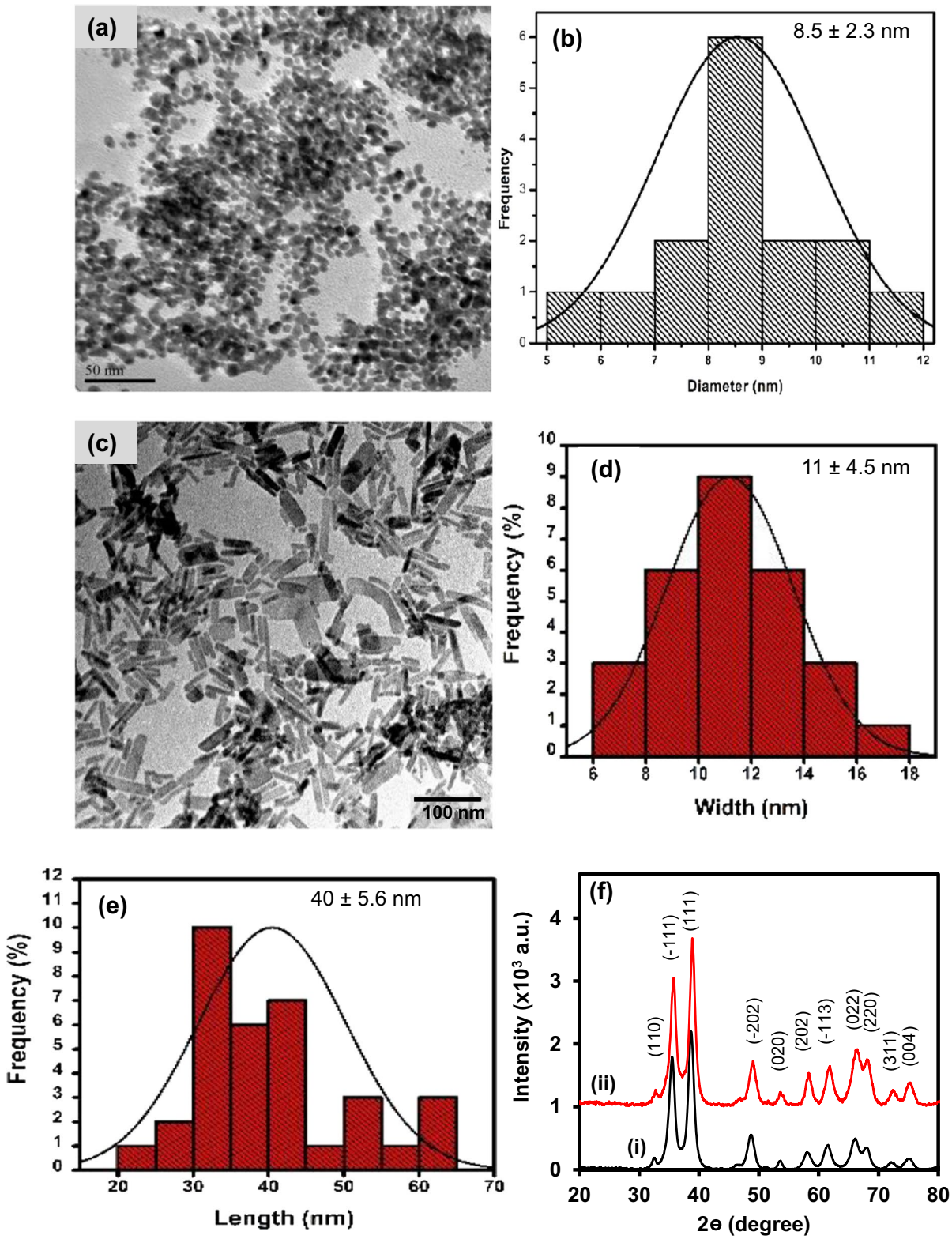

Fig. 1 TEM micrographs for (**a**) sCuONPs and (**c**) CuONRs. Histogram (size distribution) of (**b**) sCuONPs and for CuONRs (**d**) width and (**e**) length. (**f**) XRD pattern of (i) sCuONPs and (ii) CuONRs

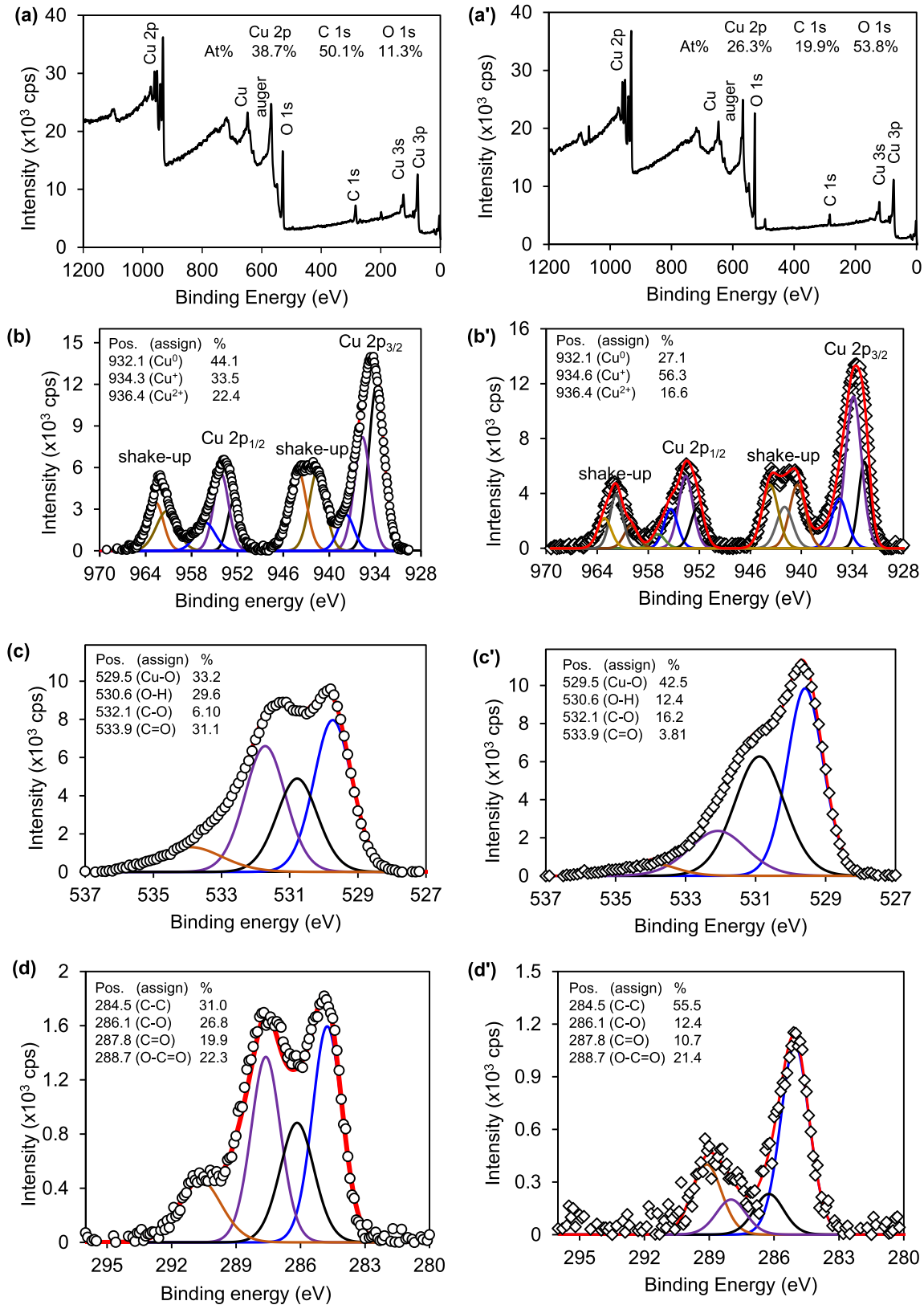
(a)
Cu 2p
Cu 2p At% 38.7%
C 1s 50.1%
O 1s 11.3%
Cu auger
O 1s
C 1s
Cu 3s
Cu 3p
Intensity (x10³ cps)
Binding Energy (eV)
(a')
Cu 2p At% 26.3%
C 1s 19.9%
O 1s 53.8%
(b)
Pos. (assign) %
932.1 (Cu⁰) 44.1
934.3 (Cu⁺) 33.5
936.4 (Cu²⁺) 22.4
Cu 2p3/2
Cu 2p1/2
shake-up
shake-up
Binding energy (eV)
(b')
932.1 (Cu⁰) 27.1
934.6 (Cu⁺) 56.3
936.4 (Cu²⁺) 16.6
(c)
529.5 (Cu-O) 33.2
530.6 (O-H) 29.6
532.1 (C-O) 6.10
533.9 (C=O) 31.1
(c')
529.5 (Cu-O) 42.5
530.6 (O-H) 12.4
532.1 (C-O) 16.2
533.9 (C=O) 3.81
(d)
284.5 (C-C) 31.0
286.1 (C-O) 26.8
287.8 (C=O) 19.9
288.7 (O-C=O) 22.3
(d')
284.5 (C-C) 55.5
286.1 (C-O) 12.4
287.8 (C=O) 10.7
288.7 (O-C=O) 21.4

◂**Fig. 2** Survey spectra of (**a**) sCuONPs and (**a'**) CuONRs and the corresponding high-resolution spectra of Cu 2p for (**b**) sCuONPs and (**b'**) CuONRs, O 1 s for (**c**) sCuONPs and (**c'**) CuONRs and C 1 s for (**d**) sCuONPs and (**d'**) CuONRs

to the composition of the sample. From the elemental composition of the survey spectra, the empirical formula of pure material and a chemical or electronic state of each element can be determined (Biesinger et al. 2010; Nagajyothi et al. 2017). The sCuONPs and CuONRs samples contained Cu 2p at 928–970 eV, C 1 s at 285 eV, and O 1 s at 532 eV. The additional peaks are due to Cu 3p (74.9 eV), Cu 3 s (122.4 eV), and Cu Auger (Cu LMM) peak at 647.5 eV. The high-resolution spectrum of Cu 2p exhibited multiple oxidation states, and the peak shape was similar to CuO with Cu^{2+} oxidation state (Biesinger et al. 2010). The Cu 2p peaks in Fig. 2b for sCuONPs and Fig. 2b' for CuONRs also showed mixed oxidation states, and three components were synthesized corresponding Cu^0 at 932.1 eV with the CuLMM confirming the metallic copper and Cu^{2+} at 934.3 eV for CuO and 936.4 eV for $Cu(OH)_2$. The high-resolution spectra of Cu 2p core-level in Fig. 2b for sCuONPs and Fig. 2b' for CuONRs showed two peaks corresponding to Cu $2p_{2/3}$ and Cu $2p_{1/2}$, respectively, indicating pure copper (II) oxide. The two peaks exist as CuO with the peak at lower binding energy Cu $2p_{3/2}$ and at high binding energy within Cu $2p_{1/2.}$ The spectra of both sCuONPs and CuONRs also showed shake-up peaks typical of Cu (II) (Mcintyre and Cook 1975), at binding energies 940.8 eV and 960.3 eV as evidence of an open $3d^9$ shell corresponding to the Cu^{2+} state (Biesinger et al. 2010; Nagajyothi et al. 2017; Mcintyre and Cook 1975; Cano et al. 2001; Salcedo and Sevilla 2013)**.** The split spin–orbit coupling (△) for the Cu $2p_{1/2}$ and Cu $2p_{3/2}$ was 19.6 eV. The corresponding elemental composition (at %) of Cu, O. C, and O are shown in the survey spectra, and oxidation states of various elements were investigated using high-resolution spectra with components synthesized. The O 1 s high-resolution core levels were investigated, and four components were synthesized for Cu–O at 529.5 eV, O–H at 530.6 eV, C-O at 532.1, and C = O at 533.9 eV for both sCuONPs in Fig. 2c and CuONRs in Fig. 2c'. The Cu–O component was very important and accounted for high concentrations for both sCuONPs (33.5%) and CuONRs (37.8%) as has been reported (Aparna et al. 2012; Turner 1988). Another component is O–H due to the hydroxyl groups from the $Cu(OH)_2$ and glacial acetic acid used in the synthesis. The other components (C-O, C = O, O-C = O) were due to –COOH from glacial acetic acid. The C 1 s high-resolution core level spectra for sCuONPs in Fig. 2d and for CuONRs in Fig. 2d' also fitted for four components and due to glacial acetic acid. The component % compositions were as displayed in the Fig. insets. These results confirm the successful synthesis of sCuONPs and CuONRs with Cu^0 and Cu^{2+} oxidation state for CuO and $Cu(OH)_2$. The characterization techniques confirmed the successful synthesis of spherical and rod-like copper oxide nanoparticles.

Peroxidase-like activity of sCuONPs and CuONRs

The peroxidase-like activity of the synthesized sCuONPs and CuONRs was evaluated by mixing the nanoparticles with H_2O_2 and TMB. The images (insert in Fig. 3) shows no color changes in the solutions containing nanoparticles alone, Fig. 3(i), and when nanoparticles are in the presence of 30 mmol. L^{-1} H_2O_2 or 1.0 mmol.L^{-1} TMB in Fig. 3(ii). When sCuONPs in Fig. 3a(iii) and CuONRs in Fig. 3b(iii) are in the presence of the 30 mmol.L^{-1} H_2O_2 and 1.0 mmol.L^{-1} TMB the solution turned blue in color.

The UV–vis absorption spectra of blue color solutions have absorption maxima at 370 nm and 652 nm. The UV–vis absorption spectra are similar to those of HRP in solution containing H_2O_2 and TMB. Therefore, the sCuONPs and CuONRs exhibit peroxidase-like activity. The intrinsic peroxidase-like activity of the nanoparticles results from the intact nanoparticles and not from the leached metal ions. The copper salt, $Cu(OAc)_2$, used for the synthesis of sCuONPs and CuONRs was investigated for peroxidase-like activity. Figure S2 (SI) shows UV–vis of $Cu(OAc)_2$ (i) alone, in the presence of (ii) 1.0 mmol.L^{-1} TMB or 30 mmol.L^{-1} H_2O_2 and (iii) 1.0 mmol.L^{-1} TMB + 30 mmol.L^{-1} H_2O_2. The UV–vis spectra did not show absorption bands at 370 nm and 652 nm, and thus no peroxidase-like activity was ascribed to the metal ions.

Conditions that affect peroxidase-like activity of CuONPs

Natural enzymes' optimum activity is affected by the extreme environmental conditions they are exposed,

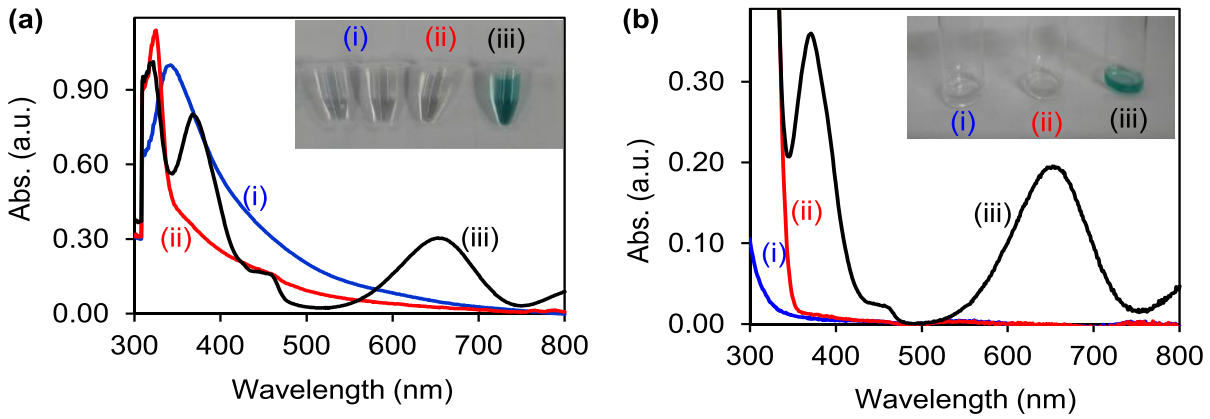

Fig. 3 UV–vis spectra of (**a**) sCuONPs and (**b**) CuONRs (i) alone, with (ii) 1.0 mmol.L^{-1} TMB or 30.0 mmol.L^{-1} H_2O_2, and with (iii) 1.0 mmol.L^{-1} TMB + 30 mmol.L^{-1} H_2O_2. (Inset color changes as per the solutions)

such as pH and temperature. The extreme environmental conditions lead to enzymes denaturing and losing activity. According to the literature, HRP was reported to be acid pH dependent and have maximum activity between 35 and 45 °C (Tatzber et al. 2003; Wei and Wang 2013; Wang 2001). Also HRP require low concentrations of H_2O_2 to reach maximum enzyme activity because high concentrations of H_2O_2 inhibit and saturate the enzyme active center leading to a loss of enzyme activity (Tatzber et al. 2003; Wei and Wang 2013; Wang 2001). Therefore, the effect of pH, temperature, and H_2O_2 concentration was investigated to see the environmental effect on the peroxidase-like activity of the synthesized sCuONPs and CuONRs. At pH 5, the absorption was the highest for both nanoparticles, sCuONPs in Fig. 4a and CuONRs in Fig. 4a'. Therefore, pH 5 was chosen as the optimum pH. The decrease in absorption bands as the pH increases is due to the fact that H_2O_2 is not stable in alkaline conditions. The H_2O_2 in basic conditions is converted to form molecular oxygen and water molecules (Torres et al. 2014). This occurs before the production of reactive oxygen radical species for TMB oxidation. H_2O_2 is catalyzed by the nanoparticle to produce reactive oxygen radical species (ROS) such as $HO^{\bullet-}$, $HOO^{\bullet-}$ and $O_2^{\bullet-}$ similar a well-known Fenton reaction (Heckert et al. 2008). ROS are responsible for oxidation of TMB to blue colored products. The catalytic reaction was effected by the oxygen vacant sites on the surface of the nanoparticles with Cu^{+} and Cu^{2+} species as confirmed by XPS experiment. The production of ROS will be investigated later by chemical approach using 1,3-diphenylisobenzofuran (DPBF) as a radical quencher. The reaction mechanism steps for the reduction of H_2O_2 by nanoparticles occurs in two steps: (i) H_2O_2 adsorbs onto the nanoparticle surface via the oxygen or hydrogen atom and (ii) the O–O, O–H bonds of H_2O_2 breaks catalytically to form ROS ($HO^{\bullet-}$, $HOO^{\bullet-}$ and $O_2^{\bullet-}$) (Qiao et al. 2014). The absorbance at 650 nm increased linearly with increasing time for color development. At about 10 min, it deviated from linearity, and a plateau was observed at 18 min for sCuONPs, in Fig. 4b. For CuONRs in Fig. 4b', the deviation from linearity occurred at about 8 min, and the plateau was observed at 16 min. Testing the effect of temperature was also investigated, and the increase in absorption at 652 nm was monitored. Figure 4c for sCuONPs showed local maximum between 40 and 50 °C, but the absorption increased further even at temperatures above 60 °C. For CuONRs, the temperature increased up to 40 °C and remained high even above 60 °C in Fig. 4c'. Therefore, the first optimum temperature of sCuONPs for reduction of H_2O_2 to generate the ROS capable of oxidizing TMB was 40 °C due to high absorption intensities, and this is close to 38 °C optimum for HRP (Song et al. 2010). The effect of H_2O_2 concentration in Fig. 4d for sCuONPs and Fig. 4d' for CuONRs showed linear relationship with the absorption intensity at 652 nm. Compared to the H_2O_2 concentration on HRP studies (Tatzber et al. 2003; Wang 2001), the nanoparticles required higher H_2O_2 concentration to reach saturation. For sCuONPs

in Fig. 4d, the linear plot was obtained for concentrations ranging from 5.0 to 50 mM with regression correlation (R^2) of 0.990 and 0.996 for CuONRs in Fig. 4d'. The HRP enzyme activity at high H_2O_2 concentration was reported (Tatzber et al. 2003) to be saturated and denature. Nanoparticles were more stable at high H_2O_2 concentration. The comparative study of the steady-state kinetics investigated and compared to the HRP confirmed stable peroxidase-like activity of nanoparticles. The nanomaterials showed excellent peroxidase-like activity even at high temperatures better than the peroxidase enzymes.

Confirmation of reactive oxygen radical species (ROS) generation

The mechanism of nanoparticle enzyme-like activity is dependent of the reduction of H_2O_2 to produce reactive oxygen radical species such as $HO^{\bullet-}$, $HOO^{\bullet-}$ and $O_2^{\bullet-}$. The generation of the reactive oxygen radical species was investigated using 1,3-diphenylisobenzofuran (DPBF), the radical scavenger. DPBF is commonly used as a singlet oxygen quencher (Tada and Baptista 2015; Zugle et al. 2011; Mvango and Mashazi 2019), and in our previous work, we demonstrated its use as a radical scavenger (Mvango and Mashazi 2019). Radicals have the same reactivity as singlet oxygen, and they are all reactive oxygen species. The degradation of DPBF can be monitored using UV–vis spectroscopy. The UV–vis spectra exhibited a peak at 417 nm due to DPBF absorption Fig. S3(ii) (SI) and 337 nm sCuONPs absorption shown in Fig. S3(a)(i) (SI) and broad peak at 345 nm for CuONRs in Fig. S3(b)(i) (SI). The changes in DPBF absorption intensity were observed in the presence of sCuONPs (Fig. 5a). The rate of degradation was more pronounced in the presence of DPBF, sCuONPs and H_2O_2, in Fig. 5b. In the presence of CuONRs, in Fig. S4, the results for the degradation of DPBF in the presence of (a) CuONRs and (b) CuONRs + H_2O_2 followed the similar trends. Figure 5c(i) shows no significant decrease in DPBF signal in the presence of H_2O_2, and the rate of degradation was 0.0013 min^{-1}. In the presence of sCuONPs, the rate of degradation of DPBF increased to 0.0084 min^{-1} in Fig. 5c(ii), and this further increased to 0.0488 min^{-1} after sCuONPs and H_2O_2 were mixed with DPBF in Fig. 5c(iii). In the presence of CuONRs, the rate of DPBF degradation was 0.0098 min^{-1} in Fig. 5d(i), and this value increased to 0.0275 min^{-1} for CuONRs and H_2O_2 were present in DPBF solution in Fig. 5d(ii). The highest rates of DPBF degradation were observed when the nanoparticles were in a mixture with H_2O_2. This was attributed to the generation of reactive oxygen radical species when the nanoparticles reduce H_2O_2 to produce reactive oxygen radical species ($HO^{\bullet-}$, $HOO^{\bullet-}$, and $O_2^{\bullet-}$). DPBF reacts in 1,4-cycloaddition reaction with the radicals (Zugle et al. 2011), and this is monitored by the decrease in the absorption peak intensity at 417 nm.

The mechanism of nanoparticle enzyme-like activity is dependent of the reduction of H_2O_2 to produce reactive oxygen radical species such as $HO^{\bullet-}$, $HOO^{\bullet-}$ and $O_2^{\bullet-}$. The generation of the reactive oxygen radical species was investigated using 1,3-diphenylisobenzofuran (DPBF), the radical scavenger. DPBF is commonly used as a singlet oxygen quencher (Tada and Baptista 2015; Zugle et al. 2011; Mvango and Mashazi 2019), and in our previous work, we demonstrated its use as a radical scavenger (Mvango and Mashazi 2019). Radicals have the same reactivity as singlet oxygen, and they are all reactive oxygen species. The degradation of DPBF can be monitored using UV–vis spectroscopy. The UV–vis spectra exhibited a peak at 417 nm due to DPBF absorption Fig. S3(ii) (SI) and 337 nm sCuONPs absorption shown in Fig. S3(a)(i) (SI) and broad peak at 345 nm for CuONRs in Fig. S3(b)(i) (SI). The changes in DPBF absorption intensity were observed in the presence of sCuONPs (Fig. 5a). The rate of degradation was more pronounced in the presence of DPBF, sCuONPs and H_2O_2, in Fig. 5b. In the presence of CuONRs, in Fig. S4, the results for the degradation of DPBF in the presence of (a) CuONRs and (b) CuONRs + H_2O_2 followed the similar trends. Figure 5c(i) shows no significant decrease in DPBF signal in the presence of H_2O_2, and the rate of degradation was 0.0013 min^{-1}. In the presence of sCuONPs, the rate of degradation of DPBF increased to 0.0084 min^{-1} in Fig. 5c(ii), and this further increased to 0.0488 min^{-1} after sCuONPs and H_2O_2 were mixed with DPBF in Fig. 5c(iii). In the presence of CuONRs, the rate of DPBF degradation was 0.0098 min^{-1} in Fig. 5d(i), and this value increased to 0.0275 min^{-1} for CuONRs and H_2O_2 were present in DPBF solution in Fig. 5d(ii). The highest rates of DPBF degradation were observed when the

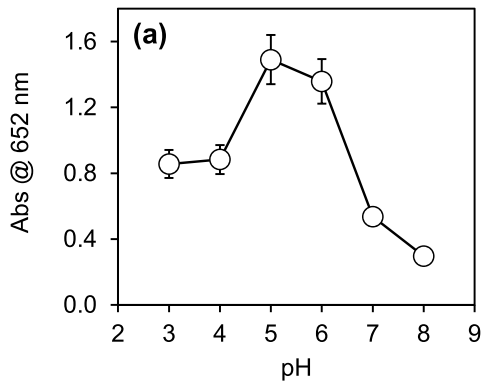
(a)
Abs @ 652 nm
pH

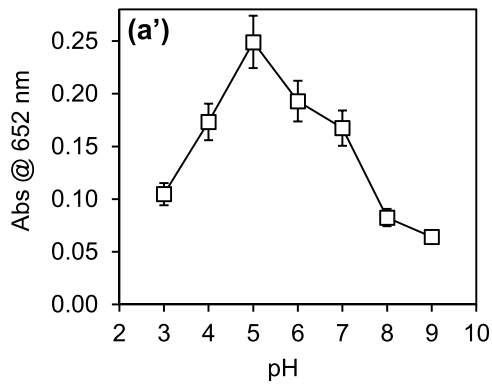
(a')
Abs @ 652 nm
pH

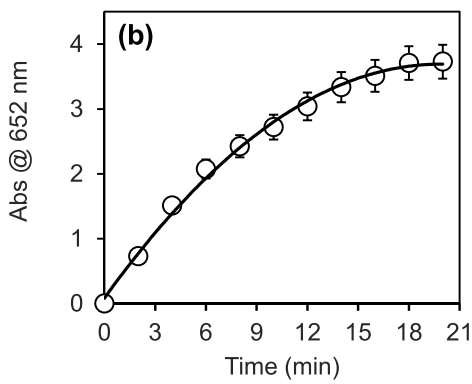
(b)
Abs @ 652 nm
Time (min)

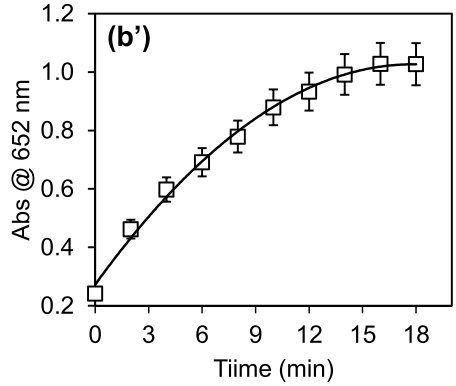
(b')
Abs @ 652 nm
Tiime (min)

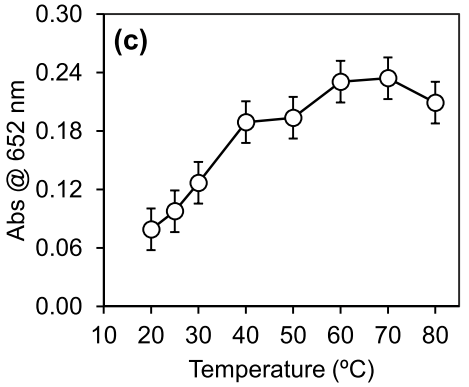
(c)
Abs @ 652 nm
Temperature (ºC)

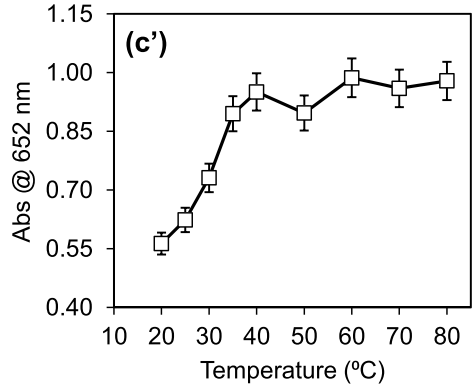
(c')
Abs @ 652 nm
Temperature (ºC)

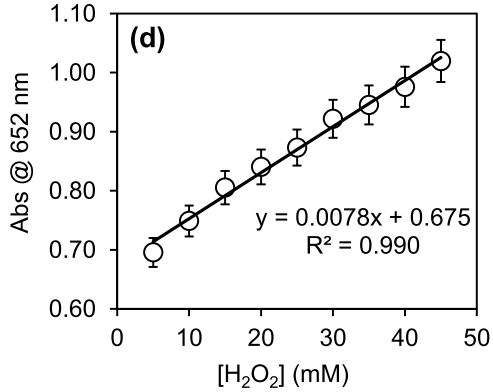
(d)
y = 0.0078x + 0.675
R² = 0.990
Abs @ 652 nm
[H2O2] (mM)

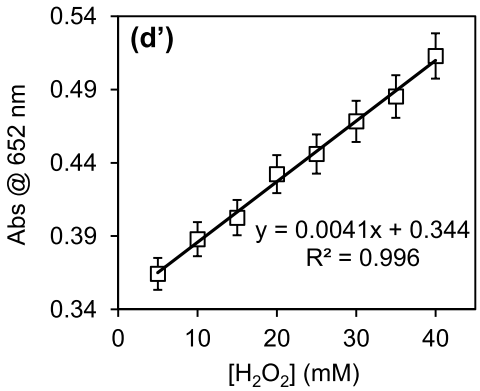
(d')
y = 0.0041x + 0.344
R² = 0.996
Abs @ 652 nm
[H2O2] (mM)

◀ **Fig. 4** The effect of pH for (**a**) sCuONPs and (**a'**) CuONRs, time for blue color development for (**b**) sCuONPs and (**b'**) CuONRs, temperature for (**c**) sCuONPs and (**c'**) CuONRs and H_2O_2 concentration for (**d**) sCuONPs and (**d'**) CuONRs on the enzymatic activity of nanoparticles

nanoparticles were in a mixture with H_2O_2. This was attributed to the generation of reactive oxygen radical species when the nanoparticles reduce H_2O_2 to produce reactive oxygen radical species ($HO^{\bullet -}$, $HOO^{\bullet -}$, and $O_2^{\bullet -}$). DPBF reacts in 1,4-cycloaddition reaction with the radicals (Zugle et al. 2011), and this is monitored by the decrease in the absorption peak intensity at 417 nm.

The radicals then react with DPBF to form 1,2-dibenzoylbenzene and its alcohol derivatives (Mayeda and Bard 1973). The nature of the radical species was not investigated due to limited access to techniques that could be used. The use of DPBF was to confirm that the mechanism of TMB oxidation was due to the catalytic reduction of H_2O_2 by the nanoparticles and producing reactive oxygen radical ($HO^{\bullet -}$, $HOO^{\bullet -}$, and $O_2^{\bullet -}$) species. The EPR measurements were also investigated. TEMP was used to measure the presence of ROS produced by the sCuONPs and CuONRs as shown in Fig. S5(SI). CuONPs with TEMP, CuONPs with H_2O_2, and H_2O_2 with TEMP in Fig. S5(i) did not show an EPR signal. The presence of the EPR signal was observed when CuONPs with H_2O_2 and TEMP were in solution (Fig. S5(ii)). This confirmed the generation of ROS supporting the results by DPBF in Fig. 5. The EPR signal was generated when a spin-trap TEMP reacted with the ROS to produced TEMPO and a signature triplet line pattern resulted as shown in Fig. S5(ii).

Steady-state kinetics of sCuONPs and CuONRs

The Michaelis–Menten model monitors the rate of enzyme–substrate interaction with varying concentrations. This model was used to study the catalytic properties of CuONPs as potential substituents for horse-radish peroxidase enzyme. The plot of initial velocity (V_0) against the concentration of H_2O_2 increase up to 6.0 mmol.L^{-1} for H_2O_2 in Fig. 6a for sCuONPs and a plateau formed afterwards. The plateau was observed around 12.0 mmol.L^{-1} of H_2O_2 for CuONRs in Fig. 6a'. For TMB, the plateau was observed at 5.0 mmol.L^{-1} for sCuONPs in Fig. 6b and around 4.0 mmol.L^{-1} for CuONRs in Fig. 6b'. The kinetics data was plotted to fit Michaelis–Menten Eq. (1):

$$V_0 = \frac{V_{max}[S]}{(K_m + [S])} \tag{1}$$

where V_0 is the initial velocity, *[S]* is the concentration of the substrate (H_2O_2 or TMB), K_m is the Michaelis–Menten constant, and V_{max} is the maximum reaction velocity. The double reciprocal (Lineweaver–Burk) plot results in a straight line and represented by Eq. (2) below:

$$\frac{1}{V_0} = \frac{K_m}{V_{max}}\frac{1}{[S]} + \frac{1}{V_{max}} \tag{2}$$

The double reciprocal plots as insets in Fig. 6 were used to calculate the K_m values from the slope of the straight line and V_{max} values from the y-intercept. The K_m was 0.14 mmol.L^{-1} and V_{max} was 1.08×10^{-8} mmol.L^{-1}.s^{-1} for sCuONPs with H_2O_2. For CuONRs with H_2O_2, the K_m was 3.15 mmol.L^{-1} and V_{max} was 4.26×10^{-8} mmol.L^{-1}.s^{-1}. The K_m for TMB was 3.29 mmol.L^{-1} for sCuONPs with a V_{max} of 1.75×10^{-9} mmol.L^{1}.s^{-1}, and for CuONRs the K_m was 3.76 mmol.L^{-1} with a V_{max} of 1.93×10^{-8} mmol.L^{-1}.s^{-1}. The K_m values were smaller for sCuONPs when compared to the CuONRs, and small K_m values indicate strong interaction of sCuONPs with substrates (TMB and H_2O_2). The V_{max} values were also of the order of magnitude smaller for sCuONPs (10^{-9} mmol.L^{-1}.s^{-1}) than for CuONRs (10^{-8} mmol.L^{-1}.s^{-1}). For the kinetic parameters for HRP (Tatzber et al. 2003; Wang 2001), the K_m values ranged from 0.214 to 3.70 mmol.L^{-1} for H_2O_2 and 0.275 to 0.434 mmol.L^{-1} for TMB. In comparison to the sCuONPs, the K_m values were smaller indicating a strong interaction of H_2O_2 with sCuONPs, but for TMB the K_m values were within the range for HRP. The V_{max} value for sCuONPs (10^{-8} mmol.L^{-1}.s^{-1}) was within the range for HRP (10^{-8} mmol.L^{-1}.s^{-1}), and for CuONRs, the V_{max} value was higher by an order of magnitude to 10^{-9} mmol.L^{-1}.s^{-1}.

Enzyme kinetics of glucose and glucose oxidase (GOx) enzyme and CuO nanoparticles

Figure 7 shows the variation of initial velocity (V_0) versus glucose concentrations for (a) sCuONPs and

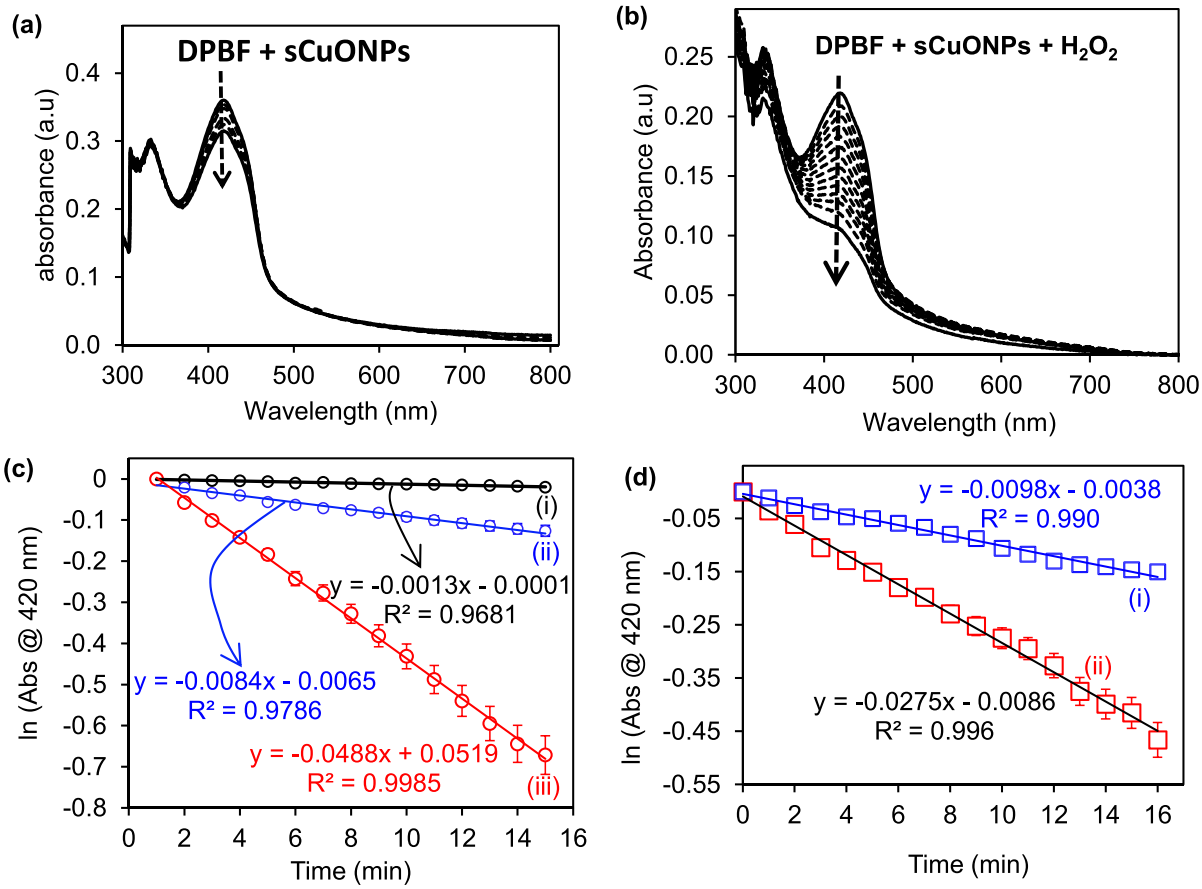

Fig. 5 UV–vis spectra for the degradation of DPBF in the presence of (**a**) sCuONPs and (**b**) sCuONPs + H_2O_2, and rate of degradation plots (**c**) (i) DPBF + H_2O_2, (ii) sCuONPs + DPBF, (iii) sCuONPs + DPBF + H_2O_2 and (**d**)(i) CuONRs + DPBF and (ii) CuONRs + DPBF + H_2O_2

(b) CuONRs. A linear increase in the initial velocity with increasing glucose concentrations up to 60 µmol.L^{-1} for sCuONPs, in Fig. 7a was observed. For CuONRs, a linear increase was observed up to 40 µmol.L^{-1} in Fig. 7b. A plateau was observed and this was typical of data representing Michaelis–Menten model and fitted well as shown in Fig. 7a and a'. The Lineweaver–Burk (double reciprocal) plot, in Fig. 7b for sCuONPs and in Fig. 7b' for CuONRs, was linear within the studied concentration range. The Lineweaver–Burk plot was used to calculate Michaelis–Menten parameters, V_{max} from the y-intercept and K_m from the slope. The V_{max} value was 3.13×10^{-7} mmol.L^{-1}.s^{-1} for sCuONPs, and for CuONRs, the V_{max} was found to be 1.48×10^{-8} mmol.L^{-1}.s^{-1}. The K_m values for sCuONPs was 0.304 mmol.L^{-1} and for CuONRs was 0.052 mmol.L^{-1}. The smaller K_m values confirmed the strong interaction between GOx enzyme and glucose substrate, and CuONRs exhibited the smallest value (0.052 mmol.L^{-1}) when compared with sCuONRs (0.304 mmol.L^{-1}).

Detection of glucose using glucose oxidase and CuO nanoparticles

The detection of glucose was evaluated using enzymatic oxidation reaction of glucose oxidase enzyme and D-glucose to produce hydrogen peroxide (as by-product) and gluconolactone (gluconic acid). CuONPs (spherical and anisotropic rod-like nanoparticles) were then introduced after the glucose oxidation reaction, and this resulted in the oxidation of hydrogen peroxide and production of ROS. In the

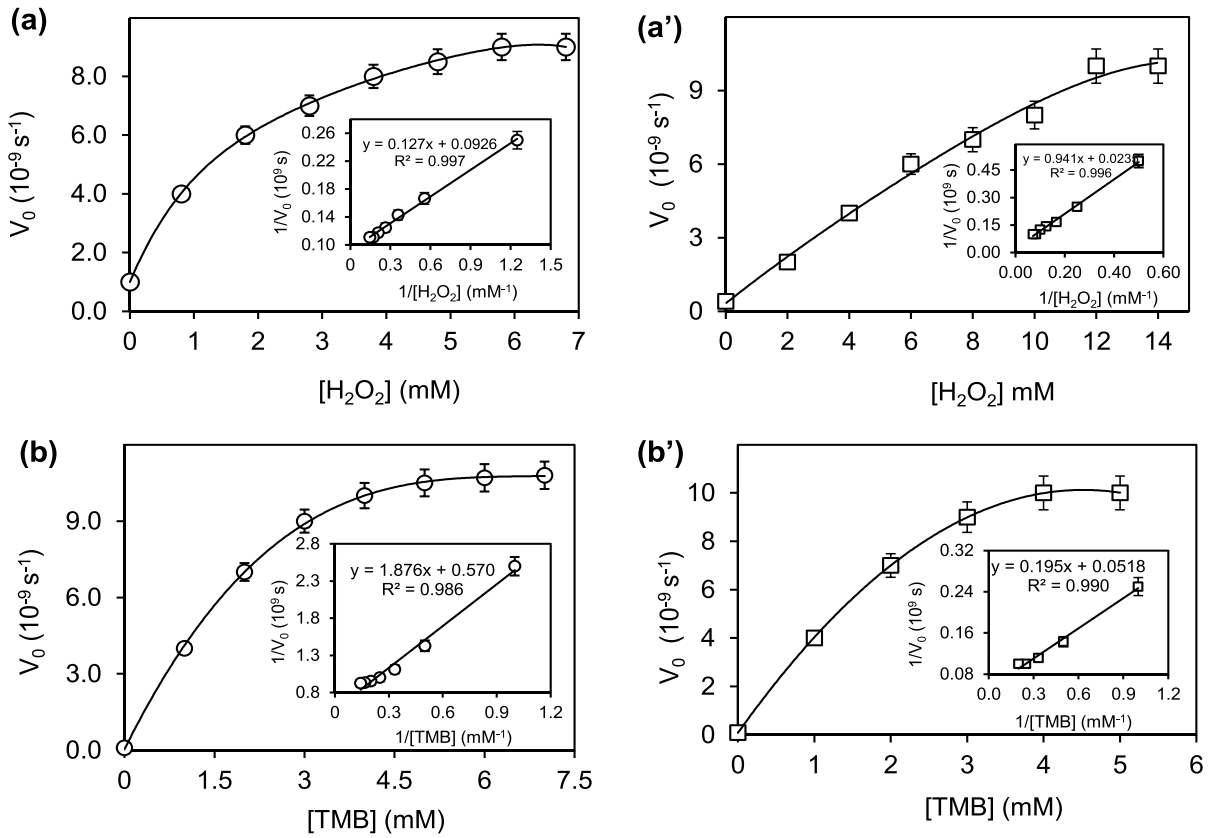

Fig. 6 Variation of rate (velocity) vs the concentrations of H_2O_2 (**a**) sCuONPs and (**a'**) CuONRs and for TMB (**b**) sCuONPs and (**b'**) CuONRs. Inset: double reciprocal (Lineweaver–Burk) plots

presence of TMB, blue colored products formed, and this was due to the oxidized TMBDI (diimine charge-transfer complex) with absorption maxima at 652 nm and 370 nm. The variation of glucose concentration was monitored spectrophotometrically. Figure 8 shows an increase in UV–vis spectra and their corresponding calibration curves for increasing glucose concentrations for (a) sCuONPs and (b) CuONRs. For sCuONPs, the response was linear up to 70 µmol.L^{-1} with the limit of detection (LoD) of 2.43 µmol.L^{-1}. The linear range for CuONRs was up to 40 µmol.L^{-1} and the detection limit of 3.55 µmol.L^{-1}. The limit of detection of glucose was obtained from the linear regression analysis in Fig. 8a' and b' calculated using 3σ (σ standard deviation of the blank sample). In Fig. 8b', the point at 5 µmol.L^{-1} was excluded from the linear calibration curve as it resided above the linear curve. The LoD values are within the reported values for different shape copper oxide nanoparticles for electrochemical measurements. The stability of the evaluated system depends on CuO nanoparticles and these exist in powder form. CuONPs have long shelf-life and remain catalytically active. The other materials used for biosensing, that is, glucose oxidase enzyme, D-glucose, hydrogen peroxide, and chromagen (TMB), are to be freshly prepared before use. Various copper nanomaterials with different morphology have been reported for glucose detection and are summarized in the review article by El-Safty and Shenashen 2020 (El-Safty and Shenashen 2020). The majority of the methods are based on the non-enzymatic electrochemical detection of glucose. In this work colorimetric detection of glucose afforded a naked eye readout with the blue color development. The quantification was accomplished using UV–vis spectrophotometer. The effect of morphology and size was not clearly visible as sCuONPs and CuONRs gave similar LoD values for the detection of glucose

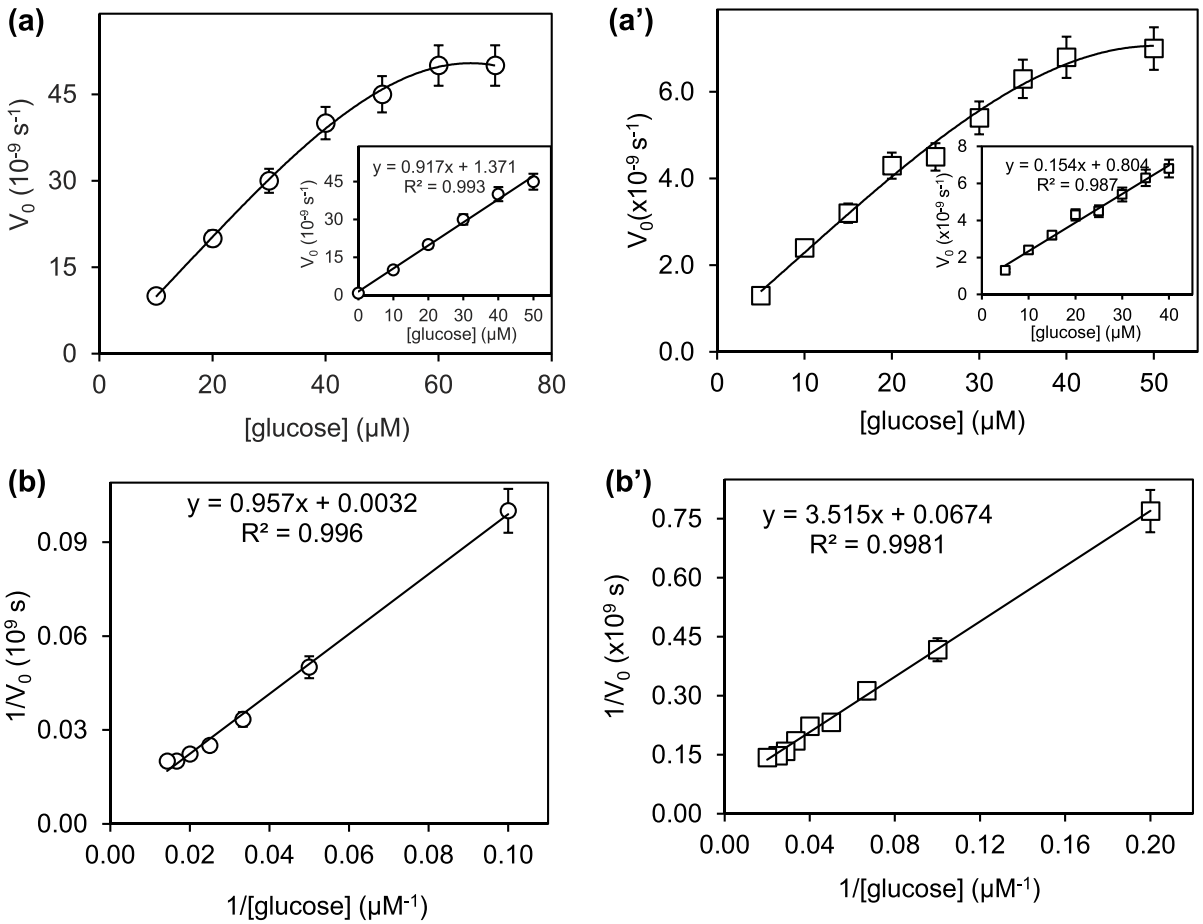

Fig. 7 Steady-state kinetic plots of initial velocity (V_0) vs [glucose] for (**a**) sCuONPs and (**a'**) CuONRs and their double reciprocal (Lineweaver–Burk) plots for (**b**) sCuONPs and (**b'**) CuONRs. Constant TMB concentrations (5.0 mmol.L^{-1} for sCuONPs and 4.0 mmol.L^{-1} CuONRs) and GOx (5.0 μg. mL^{-1}). Insets in (**a**) and (**a'**) are the linear plots of V_0 vs [glucose]

in μmol.L^{-1} similar to the reported in literature. The sensitivity values for the detection of glucose were also similar for sCuONPs (3.1 a.u.nmol.L^{-1}) and for CuONRs was 3.6 a.u.nmol.L^{-1}.

Selectivity towards glucose

The selectivity and specificity towards β-D-glucose is ascribed to the use of glucose oxidase (GOx) enzyme. GOx converts β-D-glucose to gluconic acid and produce H_2O_2 as by-product (Wang et al. 2019). H_2O_2 is catalytically converted to ROS species (as demonstrated above). ROS oxidizes TMB (3,3′,5,5′-tetramethylbenzidine) to blue colored TMBDI (3,3′,5,5′-tetramethylbenzidiimine) products. Figure 9 shows UV–vis spectra and corresponding bar chart which shows the signal due to the 0.10 mM of (i) β-D-glucose, (ii) uric acid, and (iii) ascorbic acid in (a) sCuONPs and (b) CuONRs. If glucose is replaced with ascorbic acid, uric acid, paracetamol, or dopamine, there was no color change, and very small UV–vis absorption signal was observed. The absorption spectra of all the interfering species gave background (very small) signal compared to β-D-glucose at 0.10 mM concentration. This confirms that the studied interfering species do not get oxidized by GOx enzyme and not produce H_2O_2. This study confirms selectivity towards glucose.

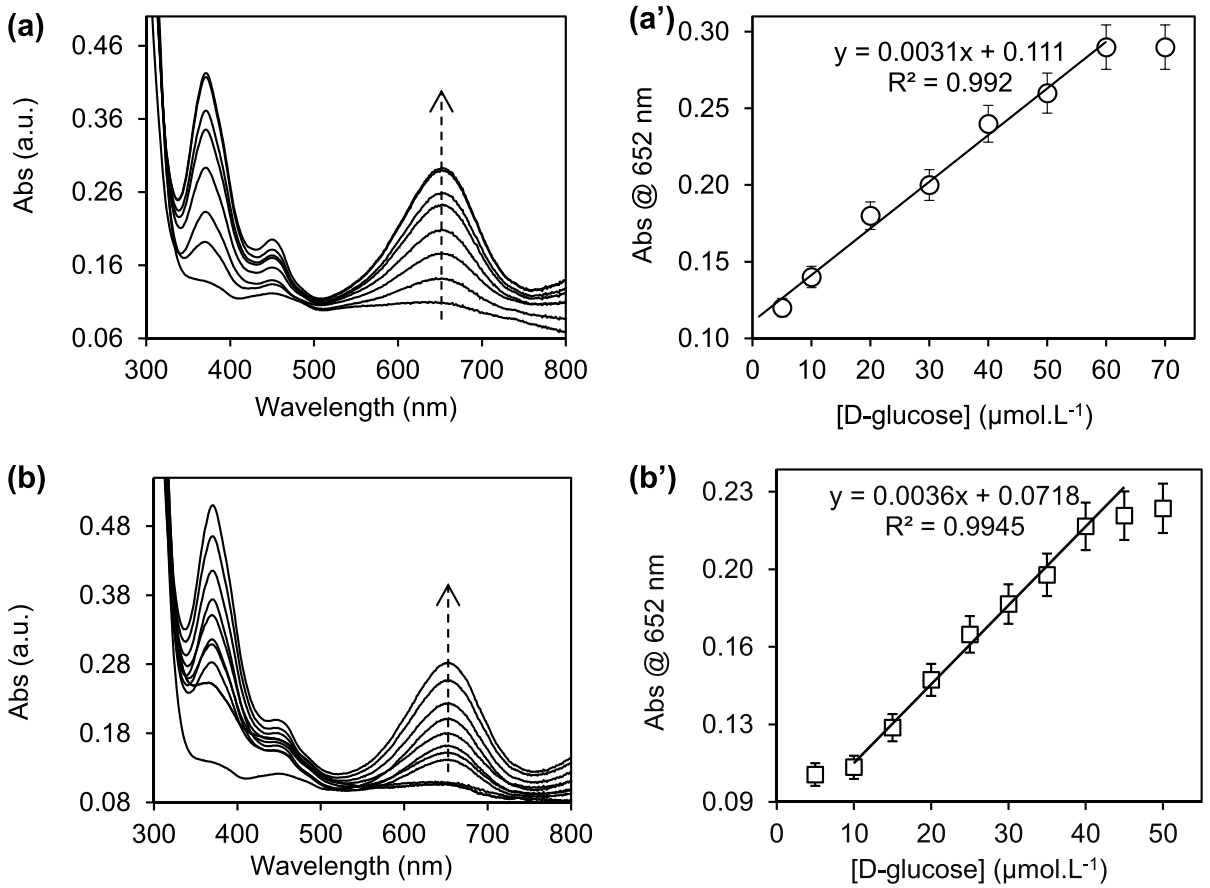

Fig. 8 UV–vis spectra and their corresponding calibration curves for increasing glucose concentrations for (**a**) sCuONPs and (**b**) CuONRs

Conclusions

The synthesis and the characterization of the spherical and rod-like CuO nanoparticles were successful and confirmed using microscopic and spectroscopic techniques. The TEM images confirmed the spherical nanoparticles with 8.5 ± 2.3 nm diameter. The nanorods (CuONRs) had 11 ± 4.5 nm diameter (width) and 40 ± 5.6 nm length. The XPS survey spectra confirmed the presence of copper (Cu 2p) and oxygen (O 1 s) species due to CuO nanoparticles and C 1 s from the citric acid. The core-level high resolution spectra of Cu 2p confirmed that both the nanoparticles contained mixed (Cu^0, Cu^+, and Cu^{2+}) oxidation states with strong shake-up peaks at high binding energies. The oxygen core-level high-resolution spectra confirmed different chemical oxidation states for oxygen, lattice oxygen (Cu–O), O–H, C-O, and C = O. The lattice oxygen (Cu–O) was a dominant component for both copper oxide nanoparticles. The nanoparticles both exhibited peroxidase-like activity when in solution containing H_2O_2 and TMB with strong absorption maxima at 652 nm and 370 nm similar to the HRP in similar solutions. The effect of various conditions was studied and confirmed that the nanoparticles have strong absorption at pH 5; the color development was highest after 16 min. The nanoparticles exhibited high peroxidase-like activity even at temperatures between 40 and 80 °C, and the peroxidase-like activity was linear with increasing H_2O_2 concentrations. The excellent peroxidase-like activity at temperature above 40 °C confirms that copper oxide nanoparticles can replace HRP enzyme in enzyme-based immunoassays. HRP has narrow pH and temperature for optimum enzyme activity. The enzymatic properties followed Michaelis–Menten

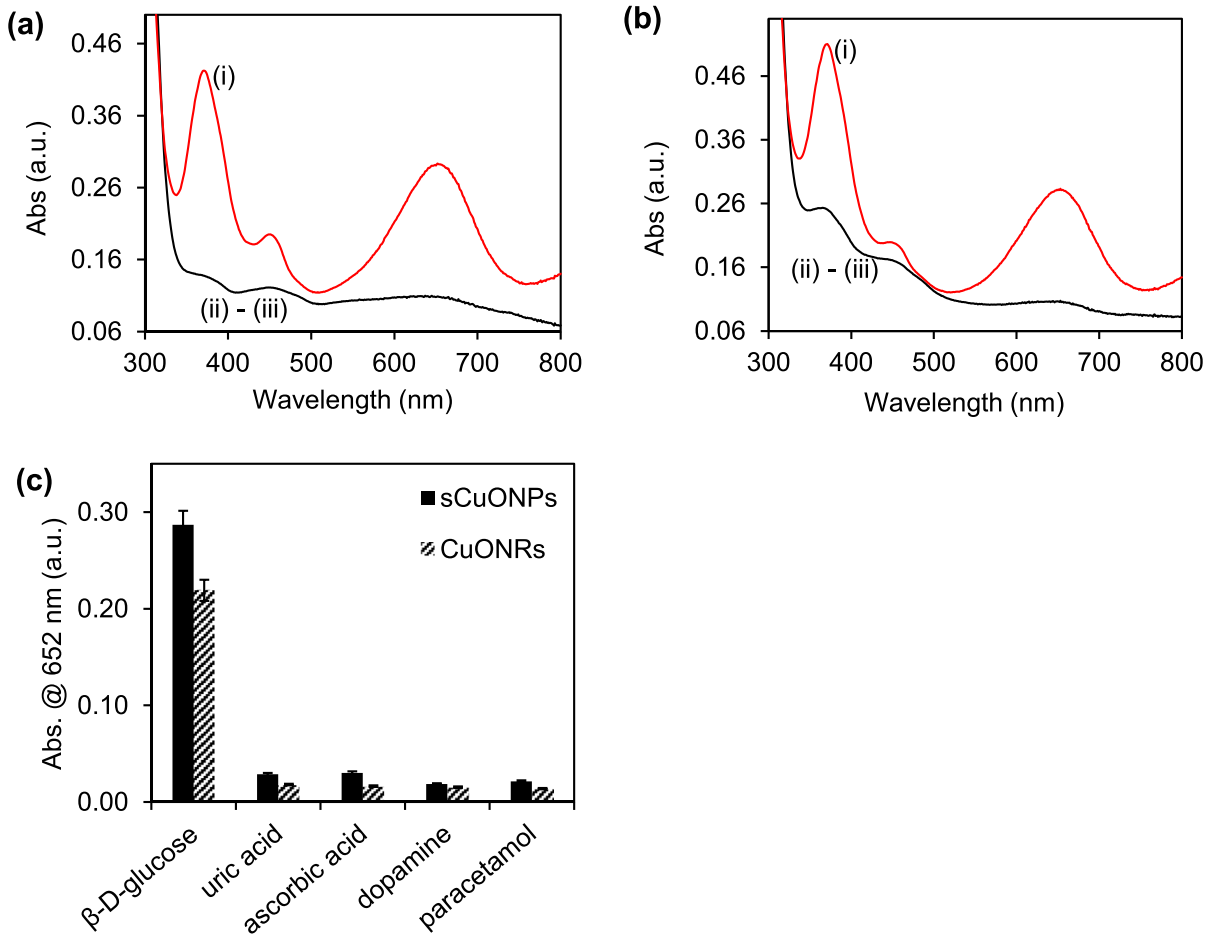

Fig. 9 UV–vis spectra and corresponding bar chart which shows the signal due to the 0.10 mM presence of (i) β-D-glucose, (ii) uric acid and (iii) ascorbic acid in (**a**) sCuONPs and (**b**) CuONRs

kinetics with K_m values for H_2O_2 of 0.14 mmol.L^{-1} for sCuONPs and 3.15 mmol.L^{-1} for CuONRs. For TMB, the K_m values were 3.29 mmol.L^{-1} for sCuONPs and 3.76 mmol.L^{-1} for CuONRs. These values are within the range for HRP, and for sCuONPs, the K_m (0.14 mmol.L^{-1}) value confirmed strong interaction between the nanoparticles and H_2O_2 substrate. The copper nanoparticles were successfully used for colorimetric detection of glucose. The limit of detection (LoD) was 2.43 µmo.L^{-1} for sCuONPs and 3.55 µmo.L^{-1} for CuONRs. The linear concentration (LCR) range of sCuONPs was 0.0–60 µmo.L^{-1}, and for CuONRs, the LCR was 0.0–40 µmo.L^{-1}. The sCuONPs and CuONRs have potential for applications as substitutes for HRP enzyme in the colorimetric detection of glucose.

Author contribution S. Sicwetsha and S. Mvango: conceptualization, investigation, data curation, methodology, writing — original draft — investigation, formal analysis, validation. T. Nyokong: resources, funding acquisition, writing — review and editing. P. Mashazi: conceptualization, validation, project administration, supervision, funding acquisition, writing — review and editing.

Funding This research was funded by the South African Medical Research Council under a Self-Initiated Research Grant (MRC-SIR); National Research Foundation through Research Development Grant for Y-Rated Grant (UID 116331), NRF-STINT Bilateral (UID 118725), Rated Incentive funding (UID 96001), and Rhodes University through Sandisa Imbewu and Researcher Development Grant. SS thanks NRF for an MSc scholarship, and SM thanks DST/Mintek NIC for an MSc Scholarship.

Declarations

Consent for publication All authors agree to publish this work in Journal of Nanoparticle Research.

Conflict of interest The authors declare no competing interests.

References

André R, Natálio F, Humanes M, Leppin J, Heinze K, Wever R, Schröder HC, Müller WEG, Tremel W (2011) V_2O_5 nanowires with an intrinsic peroxidase-like activity. Adv Funct Mater 21:501–509. https://doi.org/10.1002/adfm.201001302

Aparna Y, Rao KV, Srinivasa Subbarao P (2012) Synthesis and characterization of CuO nano particles by novel sol-gel method, 2nd Int Conf Environ Sci Biotechnol 48 156–160

Biesinger MC, Lau LWM, Gerson AR, Smart RSC (2010) Resolving surface chemical states in XPS analysis of first row transition metals, oxides and hydroxides: Sc, Ti, V, Cu and Zn. Appl Surf Sci 257:887–898. https://doi.org/10.1016/j.apsusc.2010.07.086

Cano E, Torres CL, Bastidas JM (2001) An XPS study of copper corrosion originated by formic acid vapour at 40% and 80% relative humidity. Mater Corros 52:667–676. https://doi.org/10.1002/1521-4176(200109)52:9%3c667::aid-maco667%3e3.0.co;2-h

Chen H, Zhao G, Liu Y (2013) Low-temperature solution synthesis of CuO nanorods with thin diameter. Mater Lett 93:60–63. https://doi.org/10.1016/j.matlet.2012.11.055

Chen W, Chen J, Feng Y-B, Hong L, Chen Q-Y, Wu L-F, Lin X-H, Xia X-H (2012) Peroxidase-like activity of water-soluble cupric oxide nanoparticles and its analytical application for detection of hydrogen peroxide and glucose. Analyst. 137:1706–1712. https://doi.org/10.1039/c2an35072f

El-Safty SA, Shenashen MA (2020) Advanced nanoscale build-up sensors for daily life monitoring of diabetics. Adv Mater Interfaces 7:1–31. https://doi.org/10.1002/admi.202000153

Gao D, Zhang J, Zhu J, Qi J, Zhang Z, Sui W, Shi H, Xue D (2010) Vacancy-mediated magnetism in pure copper oxide nanoparticles. Nanoscale Res Lett 5:769–772. https://doi.org/10.1007/s11671-010-9555-8

Gao L, Zhuang J, Nie L, Zhang J, Zhang Y, Gu N, Wang T, Feng J, Yang D, Perrett S, Yan X (2007) Intrinsic peroxidase-like activity of ferromagnetic nanoparticles. Nat Nanotechnol 2:577–583. https://doi.org/10.1038/nnano.2007.260

Gao Z, Xu M, Lu M, Chen G, Tang D (2015) Urchin-like (gold core)@(platinum shell) nanohybrids: a highly efficient peroxidase-mimetic system for in situ amplified colorimetric immunoassay. Biosens Bioelectron 70:194–201. https://doi.org/10.1016/j.bios.2015.03.039

Gawande MB, Goswami A, Felpin FX, Asefa T, Huang X, Silva R, Zou X, Zboril R, Varma RS (2016) Cu and Cu-based nanoparticles: synthesis and applications in catalysis. Chem Rev 116:3722–3811. https://doi.org/10.1021/acs.chemrev.5b00482

Heckert EG, Seal S, Self WT (2008) Fenton-like reaction catalyzed by the rare earth inner transition metal cerium. Environ Sci Technol 42:5014–5019. https://doi.org/10.1021/es8001508

Huang TK, Lin KW, Tung SP, Cheng TM, Chang IC, Hsieh YZ, Lee CY, Chiu HT (2009) Glucose sensing by electrochemically grown copper nanobelt electrode. J Electroanal Chem 636:123–127. https://doi.org/10.1016/j.jelechem.2009.08.011

Huo C, Ouyang J, Yang H (2014) CuO nanoparticles encapsulated inside Al-MCM-41 mesoporous materials via direct synthetic route. Sci Rep 4(1–9):3682. https://doi.org/10.1038/srep03682

Jiang LC, De Zhang W (2010) A highly sensitive nonenzymatic glucose sensor based on CuO nanoparticles-modified carbon nanotube electrode. Biosens Bioelectron 25:1402–1407. https://doi.org/10.1016/j.bios.2009.10.038

Johan MR, Suan MSM, Hawari NL, Ching HA (2011) Annealing effects on the properties of copper oxide thin films prepared by chemical deposition. Int J Electrochem Sci 6:6094–6104

Kshirsagar J, Shrivastava R, Adwani P (2017) Preparation and characterization of copper oxide nanoparticles and determination of enhancement in critical heat flux. Therm Sci 21:233–242. https://doi.org/10.2298/tsci140619026k

Li C, Su Y, Zhang S, Lv X, Xia H, Wang Y (2010) An improved sensitivity nonenzymatic glucose biosensor based on a Cu_xO modified electrode. Biosens Bioelectron 26:903–907. https://doi.org/10.1016/j.bios.2010.07.007

Luo J, Jiang S, Zhang H, Jiang J, Liu X (2012a) A novel non-enzymatic glucose sensor based on Cu nanoparticle modified graphene sheets electrode. Anal Chim Acta 709:47–53. https://doi.org/10.1016/j.aca.2011.10.025

Luo L, Zhu L, Wang Z (2012b) Nonenzymatic amperometric determination of glucose by CuO nanocubes-graphene nanocomposite modified electrode. Bioelectrochemistry 88:156–163. https://doi.org/10.1016/j.bioelechem.2012.03.006

Mayeda EA, Bard AJ (1973) Production of singlet oxygen in electrogenerated radical ion electron transfer reactions. J Am Chem Soc 95:6223–6226. https://doi.org/10.1021/ja00800a012

Mcintyre NS, Cook MG (1975) X-Ray Photoelectron studies on some oxides and hydroxides of cobalt, nickel, and copper. Anal Chem 47:2208–2213. https://doi.org/10.1021/ac60363a034

Mvango S, Mashazi P (2019) Synthesis, characterization of copper oxide-gold nanoalloys and their peroxidase-like activity towards colorimetric detection of hydrogen peroxide and glucose. Mater Sci Eng C 96:814–823. https://doi.org/10.1016/j.msec.2018.12.010

Nagajyothi PC, Muthuraman P, Sreekanth TVM, Kim DH, Shim J (2017) Green synthesis: in-vitro anticancer activity of copper oxide nanoparticles against human cervical carcinoma cells. Arab J Chem 10:215–225. https://doi.org/10.1016/j.arabjc.2016.01.011

Ni P, Sun Y, Shi Y, Dai H, Hu J, Wang Y, Li Z (2014) Facile fabrication of CuO nanowire modified Cu electrode for non-enzymatic glucose detection with enhanced sensitivity. RSC Adv 4:28842–28847. https://doi.org/10.1039/c4ra03437f

Qiao F, Chen L, Li X, Li L, Ai S (2014) Peroxidase-like activity of manganese selenide nanoparticles and its analytical application for visual detection of hydrogen peroxide and

glucose. Sens Actuators B Chem 193:255–262. https://doi.org/10.1016/j.snb.2013.11.108

Reitz E, Jia W, Gentile M, Wang Y, Lei Y (2008) CuO nanospheres based nonenzymatic glucose sensor. Electroanalysis 20:2482–2486. https://doi.org/10.1002/elan.200804327

Salcedo ARM, Sevilla FB (2013) Citrate-capped gold nanoparticles as colorimetric reagent for copper(II) Ions. Philipp Sci Lett 6:90–96

Shackery I, Patil U, Pezeshki A, Shinde NM, Kang S, Im S, Jun SC (2016) Copper hydroxide nanorods decorated porous graphene foam electrodes for non-enzymatic glucose sensing, electrochim. Acta 191:954–961. https://doi.org/10.1016/j.electacta.2016.01.047

Song D, Mu Y, Liu X, Zhao L, Zhang H, Jin Q (2003) An optical immunosensor based on surface plasmon resonance for determination of bFGF. Microchem J 74:93–97. https://doi.org/10.1016/S0026-265X(02)00176-5

Song Y, Qu K, Zhao C, Ren J, Qu X (2010) Graphene oxide: intrinsic peroxidase catalytic activity and its application to glucose detection. Adv Mater 22:2206–2210. https://doi.org/10.1002/adma.200903783

Tada DB, Baptista MS (2015) Photosensitizing nanoparticles and the modulation of ROS generation. Front Chem. 3 33 (1–14). https://doi.org/10.3389/fchem.2015.00033

Tatzber F, Griebenow S, Wonisch W, Winkler R (2003) Dual method for the determination of peroxidase activity and total peroxides-iodide leads to a significant increase of peroxidase activity in human sera. Anal Biochem 316:147–153. https://doi.org/10.1016/S0003-2697(02)00652-8

Tshenkeng K, Mashazi P (2020) Covalent attachment of cobalt (II) tetra-(3-carboxyphenoxy) phthalocyanine onto pre-grafted gold electrode for the determination of catecholamine neurotransmitters, Electrochim. Acta. 137015. https://doi.org/10.1016/j.electacta.2020.137015

Torres CRG, Crastechini E, Feitosa FA, Pucci CR, Borges AB (2014) Influence of pH on the effectiveness of hydrogen peroxide whitening. Oper Dent 39:E261–E268. https://doi.org/10.2341/13-214-L

Turner NH (1988) Surface analysis: x-ray photoelectron spectroscopy and auger electron spectroscopy. Anal Chem 60:377–387. https://doi.org/10.1021/ac00163a024

Wang G, Huang J, Chen S, Gao Y, Cao D (2011) Preparation and supercapacitance of CuO nanosheet arrays grown on nickel foam. J Power Sources 196:5756–5760. https://doi.org/10.1016/j.jpowsour.2011.02.049

Wang J (2001) Glucose Biosensors 40 Years of Advances. Electroanalysis 13:983–988

Wang M, Wang D, Chen Q, Li C, Li Z, Lin J (2019) Recent advances in glucose-oxidase-based nanocomposites for tumor therapy. Small 15:1903895. https://doi.org/10.1002/smll.201903895

Wang W, Zhang L, Tong S, Li X, Song W (2009) Three-dimensional network films of electrospun copper oxide nanofibers for glucose determination. Biosens Bioelectron 25:708–714. https://doi.org/10.1016/j.bios.2009.08.013

Wang X, Hu C, Liu H, Du G, He X, Xi Y (2010) Synthesis of CuO nanostructures and their application for nonenzymatic glucose sensing. Sens Actuators B Chem 144:220–225. https://doi.org/10.1016/j.snb.2009.09.067

Wei H, Wang E (2013) Nanomaterials with enzyme-like characteristics (nanozymes): next generation artificial enzymes. Chem Sociery Rev 46:6060–6093. https://doi.org/10.1039/c3cs35486e

Yao W, Li FL, Li HX, Lang JP (2015) Fabrication of hollow Cu_2O@CuO-supported Au-Pd alloy nanoparticles with high catalytic activity through the galvanic replacement reaction. J Mater Chem a 3:4578–4585. https://doi.org/10.1039/c4ta06378c

Zhang W, Wen X, Yang S, Berta Y, Wang ZL (2003) Single-crystalline scroll-type nanotube arrays of copper hydroxide synthesized at room temperature. Adv Mater 15:822–825. https://doi.org/10.1002/adma.200304840

Zhang X, Shi W, Huang Y, Liu X (2014) Intrinsic peroxidase-like activity exhibited by cerium oxide nanoparticles and their application to glucose detection. Sci Sin Chim 44:1633–1640. https://doi.org/10.1360/n032013-00060

Zhong Y, Shi T, Liu Z, Cheng S, Huang Y, Tao X, Liao G, Tang Z (2016) Ultrasensitive non-enzymatic glucose sensors based on different copper oxide nanostructures by in-situ growth. Sens Actuators B Chem 236:326–333. https://doi.org/10.1016/j.snb.2016.06.020

Zhou S, Feng X, Shi H, Chen J, Zhang F, Song W (2013a) Direct growth of vertically aligned arrays of Cu(OH)2 nanotubes for the electrochemical sensing of glucose. Sens Actuators B Chem 177:445–452. https://doi.org/10.1016/j.snb.2012.11.035

Zhou Y, Yao YW, Qi Q, Fang Y, Li JY, Yao C (2013b) A click-activated fluorescent probe for selective detection of hydrazoic acid and its application in biological imaging. Chem Commun 49:5924–5926. https://doi.org/10.1039/c3cc40698a

Zugle R, Litwinski C, Torto N, Nyokong T (2011) Photophysical and photochemical behavior of electrospun fibers of a polyurethane polymer chemically linked to lutetium carboxyphenoxy phthalocyanine. New J Chem 35:1588–1595. https://doi.org/10.1039/c1nj20126c